L1 Antibodies Block Lymph Node Fibroblastic Reticular Matrix Remodeling In Vivo

By Gino Di Sciullo,* Tim Donahue,* Melitta Schachner,‡§ and Steven A. Bogen*

*From the *Department of Pathology and Laboratory Medicine, Boston University School of Medicine, Boston, Massachusetts 02118; the ‡Department of Neurobiology, Swiss Federal Institute of Technology, CH-8093 Zurich, Switzerland; and §Zentrum für Molekulare Neurobiologie, Universität Hamburg, D-20246 Hamburg, Germany*

Summary

L1 is an immunoglobulin superfamily adhesion molecule highly expressed on neurons and involved in cell motility, neurite outgrowth, axon fasciculation, myelination, and synaptic plasticity. L1 is also expressed by nonneural cells, but its function outside of the nervous system has not been studied extensively. We find that administration of an L1 monoclonal antibody in vivo disrupts the normal remodeling of lymph node reticular matrix during an immune response. Ultrastructural examination reveals that reticular fibroblasts in mice treated with L1 monoclonal antibodies fail to spread and envelop collagen fibers with their cellular processes. The induced defect in the remodeling of the fibroblastic reticular system results in the loss of normal nodal architecture, collapsed cortical sinusoids, and macrophage accumulation in malformed sinuses. Surprisingly, such profound architectural abnormalities have no detectable effects on the primary immune response to protein antigens.

Key words: lymph node • L1 • cell adhesion molecule • fibroblastic reticular system • architecture

Lymph nodes (LNs) can undergo rapid and profound hypertrophy during an immune response. However, the mechanisms underlying lymphoid tissue matrix remodeling remain poorly understood. Previous studies of the lymphoid reticular matrix in immune animals have largely been descriptive in nature, as it has not been possible to selectively disrupt this feature in an otherwise normal, healthy animal.

Under normal immune conditions, the integrity of the lymphoid tissue is maintained because of the adaptive nature of the reticular matrix. This matrix, termed the fibroblastic reticular system (FRS),[1] is comprised of a fibrous reticulum and associated fibroblasts (1). The reticular fibers are primarily made up of type III collagen, but also contain small amounts of elastic fibers (2), microfibrils (3), type IV collagen (4), and laminin (5). The elastic components, admixed with the collagen bundles, confer resiliency to the fibers during organ distention.

Anchored to the reticular fibers are reticular fibroblasts (RFs), which ensheathe the fibers by wrapping around them in a manner analogous to Schwann cell enclosure of axons (1, 6). The enclosure of the reticular fibers by RF cytoplasmic processes is sealed by desmosome-like junctional complexes at the juxtaposed RFs' membranes (7).

The reticular fibers and associated fibroblasts together form a three-dimensional cellular reticulum that forms the walls of sinuses and delimits compartments within the node. Based on these structural features, the FRS is believed to function primarily as (*a*) a mechanical supportive scaffolding, (*b*) a substratum for immune cell motility, and (*c*) partitions that establish immune microenvironments. It has also been hypothesized that the extracellular space formed by the RF enclosure of the reticular fibers may facilitate antigen transport between different compartments within the node (8–10).

Our studies of LN architecture began when, in the course of studying the function of the L1 cell adhesion molecule in the murine immune system, we observed structural abnormalities in LNs from mice injected with an L1 mAb. L1 is a type I transmembrane glycoprotein with an apparent molecular mass of 200 kD that is highly expressed by neural cells and tumors of neural origin (11). Although L1 was isolated and purified initially from mouse

[1]*Abbreviations used in this paper:* ANOVA, analysis of variance; CLSM, confocal laser scanning microscopy; DTH, delayed type contact hypersensitivity; FRS, fibroblastic reticular system; Mϕ, macrophage; NRIg, normal rat immunoglobulin; RF, reticular fibroblast; RT, room temperature; TEM, transmission electron microscopy.

 J. Exp. Med. © The Rockefeller University Press • 0022-1007/98/06/1953/11 $2.00
Volume 187, Number 12, June 15, 1998 1953–1963
http://www.jem.org

brain extracts, it is also expressed by a variety of nonneuronal cells. Cells of hematopoietic origin express L1 (12), as do epithelial cells of the intestine (13) and male urogenital tract (14). Of special relevance to this study, L1 expression has also been demonstrated in mouse fibroblast L cells by Western blot analysis of membrane preparations (15).

In this report, we examine the in vivo consequences of influencing the effect of L1 during an immune response in mice, using a previously described blocking rat anti–mouse L1 mAb designated 324 (11). We find that in vivo administration of the 324 anti-L1 mAb during the evolution of an immune response prevents normal remodeling of the reticular matrix of the draining popliteal LN.

Materials and Methods

Animals and Immunizations. In vivo experiments were conducted using 8–10-wk-old female BALB/CByj mice according to the following protocol. On day 0, 25 μg of KLH/CFA was injected into the right footpad of each mouse. For all structural experiments, 250 μg of antibody was injected intraperitoneally each day during days 2–5. Other studies testing the role of L1 during the early phases of in vivo lymphocyte sensitization involved injection with 300 μg of antibodies on days 0–5 and killing on day 7. In these latter experiments, antibody injection on day 0 preceded KLH/CFA immunization by 3 h. Mice were killed either on day 6 or day 7, and popliteal LNs were harvested. Animals were cared for in accordance with The Institutional Animal Care and Use Committee of Boston University School of Medicine.

mAb Preparation. Normal rat immunoglobulin (NRIg) was purified from normal rat serum (The Jackson Laboratory, Bar Harbor, ME) by HPLC using a J.T. Baker ABx semipreparative column (16). Likewise, the 324 and TIB 126 (American Type Culture Collection, Rockville, MD) hybridomas were grown as ascitic tumors in NCR/nude mice (Taconic Farms Inc., Germantown, NY), and mAbs were purified from ascites by HPLC.

Transmission Electron Microscopy. For transmission electron microscopy (TEM) studies, whole LNs were fixed in Karnovsky's 1/2 strength fixative at 4°C for >1 d. Tissues were washed with 0.1 M phosphate buffer, postfixed in 1% OsO_4 in 0.1 M phosphate buffer, stained with 2% uranyl acetate in 60% ethanol, and dehydrated through an ethanol gradient and embedded in Araldite (E.F. Fullam Inc., Latham, NY). 0.055-μm sections were examined and photographed in an electron microscope (model 300; Philips Electronics, Eindhoven, The Netherlands).

Immunohistochemistry and Immunofluorescence Microscopy. For confocal microscopy and immunohistochemical studies, LNs were embedded in OCT (Miles Inc., Elkhart, IN), snap frozen, cryosectioned, and acetone fixed. L1 expression in LN sections was detected using anti–mouse L1 hyperimmune rabbit serum, or preimmune rabbit serum diluted 1:2,000 (Covance Research Products Inc., Denver, PA). Rabbit anti–mouse laminin 1:100 was detected with biotin-conjugated goat anti–rabbit IgG diluted 1:100 (both from Sigma Chemical Co., St. Louis, MO) followed by ABC-HRP (Vector Laboratories, Inc., Burlingame, CA). Laminin staining was detected colorimetrically using 3,3′-diaminobenzidine (Sigma Chemical Co.). Macrophages were immunostained with biotin-conjugated anti–MAC-1 mAb (5C6) at 1 μg/ml.

Confocal Laser Scanning Microscopy. Confocal laser scanning microscopy (CLSM) was carried out on a CLSM microscope (Leica Microsystems, Wetzlar, Germany) equipped with an argon ion laser. The objective used was a 50× long working distance water immersion lens. Continuous series of 2 scans/μm were recombined to produce three-dimensional reconstructions of the entire thickness of the LN tissue. Anti–vimentin-Cy3 1:50 (V-9 clone; Sigma Chemical Co.) was used to stain frozen sections cut 48 μm thick, which had a post-acetone fixation thickness of 16 μm.

Secondary In Vitro Lymphoproliferation. LNs from KLH/CFA-immune mice treated with either anti-L1 or control antibodies were harvested on day 7. Lymphocytes were collected and washed twice in ice-cold HBSS, resuspended in complete media, and plated (5×10^5 cells/well) in flat-bottomed 96-well plates (Corning Glass Works, Corning, NY) containing media alone or with varying concentrations of soluble KLH (Calbiochem Corp., La Jolla, CA). Cells were cultured for 4 d, pulsed for 8 h with 1 μCi of [^{3}H]thymidine per well, and harvested using a PHD cell harvester (Cambridge Technology, Inc., Cambridge, MA). Counts were determined using a liquid scintillation counter (model 1414; Wallac, Gaithersburg, MD).

ELISA. Day 7 serum was tested for KLH-specific IgM and IgG antibodies by ELISA. Flexible PVC microtiter plates (Costar Corp., Cambridge, MA) were coated overnight at 4°C with 20 μg/ml KLH, and blocked with 4% BSA for 1 h at room temperature (RT). Between each step, plates were washed five times with PBS/0.2% Tween 20 (PBS/T). 50 μl of serum, diluted 1:100 in PBS/T, was incubated for 1 h at RT. Alkaline phosphatase–conjugated rabbit anti–mouse IgM and IgG gamma-specific antibodies (Sigma Chemical Co.) were diluted 1:1,000 in PBS/T and incubated for 1 h at RT. Colorimetric development of AP substrate (Sigma Chemical Co.) was read at 405 nm in a plate reader (Bio-Tek Instruments, Inc., Winooski, VT).

Flow Cytometry and LN Cell Enumeration. The total number of cells in the draining LNs was quantified by trypan blue dye exclusion with a hemocytometer. Lymphocyte subsets were quantified by flow cytometry (Coulter Profile; Coulter Corp., Miami, FL) using the following biotin-conjugated rat anti–mouse mAbs: ant-B220 (3A1/6.1 ATCC, TIB 146), anti-CD8 (ATCC, TIB 105), anti-CD4 (GK1.5), and anti-CD11b (5C6). FITC-avidin D cell sorter grade was used at 600 ng/ml (Vector Laboratories, Inc.). Each incubation (both the primary antibody and fluorescein-conjugated avidin) was for 45 min, at 4°C. Afterwards, cells were washed, fixed in 2% paraformaldehyde/PBS, and stored at 4°C until assayed.

Results

Model of LN Hypertrophy. To study the function of L1 in the immune system in vivo, we used a well-characterized immune response model in which subcutaneous injection of 25 μg of KLH emulsified in CFA to the hind footpad of a mouse elicits a vigorous immune response. In the preimmune animal, the draining popliteal LN is modest in size, averaging 1.1 mm in diameter (Table 1). However, by day 6 after immunization, the mean greatest-width diameter increases to 4 mm (Table 1). Since LNs are roughly spherical in shape, this change in dimension represents a 63-fold increase in organ volume (i.e., 4^3–1.1^3). Such extreme and rapid increases in organ volume must necessarily be accompanied by extensive matrix remodeling, regulated through poorly characterized mechanisms.

To elucidate the role of L1 in immune responses, we

Table 1. *Greatest-width Diameter of LN Frozen Sections*

Antibody	Mean diameter
	mm
Preimmune	1.1 ± 0.04
Postimmune day 6	
L1 mAb	4.0 ± 0.31
NRIg	4.1 ± 0.46

Greatest-width diameter of LN frozen sections from preimmune and postimmune day 6 mice. Five LNs from each group were serially cut, and the greatest-width diameter of each LN was recorded. Data represent the means ± SE. At day 6 after immunization, no statistical difference existed between the L1 mAb–treated group compared with NRIg-treated mice, as determined by analysis of variance (ANOVA).

first identified by immunofluorescent microscopy the LN cell types that express high levels of L1. In both the preimmune and KLH/CFA-elicited immune LN, cellular components of the FRS stain positively for L1 by indirect immunofluorescence. In particular, L1 immunostaining is especially prominent on fibroblastic sinus lining cells (Fig. 1 *A*). Although parenchymal lymphoid cells are reported to express L1 (12), in situ staining (Fig. 1 *A*) reveals that their level of expression is significantly lower than that of cells of the FRS.

LN Matrix Abnormalities. To study the effects of L1 mAb treatment on the cellular components of the FRS, we identified RFs by immunofluorescent microscopy, staining for the intermediate filament vimentin. Since fibroblasts express high amounts of vimentin relative to lymphoid cells (17), the cellular profile of RFs can be observed in situ. In stacked two-dimensional images from CLSM (Fig. 2, *A* and *B*), RFs appear bright white against the dark red background. The normal staining pattern of RFs is that of an intricately branching and elongated network of cellular processes that course through the LN (Fig. 2 *A*). By contrast, RFs in 324 mAb–treated mice have a stubby, retracted morphology (Fig. 2 *B*).

Under normal conditions, RFs modify the tissue matrix by depositing extracellular matrix components as they spread out and extend their cellular processes (5). Consequently, laminin colocalizes with vimentin-positive reticular structures in both naive and immune LN sections (data not shown). Therefore, we also examined reticular architecture by immunohistochemical staining for laminin. In LNs from control mice, laminin is faintly detected along long, branching reticular structures that thread through the lymphoid parenchyma (Fig. 2 *C*). Control mice in these experiments were injected with NRIg, a nonbinding negative control that yields a low background on indirect immunostaining. In contrast to the long, branching laminin filaments of control mice, L1 mAb–treated mice have short, fragmented, and stunted laminin filaments (Fig. 2 *D*). This abbreviated discontinuous pattern of laminin staining is strikingly similar to the appearance of the vimentin-bright cells in Fig. 2 *B*. The greatest differences in RF morphology, as identified by both vimentin and laminin immunostaining, were observed in the cortex and paracortex. These regions of the LN bear the greatest degree of packing and distention due to lymphocyte influx and proliferation.

RF Ultrastructural Abnormalities. To gain insight into the fine histologic structure of the FRS abnormalities induced by the L1 mAb, LNs were embedded in plastic and analyzed by light and TEM. Both NRIg (a nonbinding control) and anti-class I mAb (a binding negative control) were used as control antibodies with identical results. When RFs are viewed by TEM, they normally appear flattened, with elongated slender processes and large ovoid nuclei with peripherally condensed chromatin (1, 18, 19). The striated collagenous components of the reticular fibers are enclosed within the RF's cell processes. When the tissue is sectioned in a single plane, the cytoplasm of RFs appears typically as a double-contoured cellular profile with reticular fibers in between. These characteristic features of normal RFs are evident in an electron micrograph of a control group LN (Fig. 3, *A* and *B*). The RF envelops itself around reticular fibers, providing anchorage to matrix components (1, 6) and mechanical support for the RF cell body.

In contrast, these normal ultrastructural features of LN architecture are largely absent in LNs from animals treated with the L1 mAb (Fig. 3 *C*). In LNs from the L1 mAb–treated group, there were few distinguishable sinusoids in the cortex and paracortex. The few sinusoids that were found were lined with malformed RFs that were short, plump, and lacked the double-contour feature (Fig. 3 *C*). The absence of the double-contour morphology indicates the absence of cytoplasmic processes extending around reticular fibers. Therefore, RFs were unable to spread out on and attach to their substrate, resulting in a loss of adherence.

In fact, numerous RFs with little or no associated collagenous components were apparently sloughed into collapsed sinusoidal spaces (Fig. 4, *A* and *B*). Fig. 4 *A* (light photomicrograph) and *B* (electron photomicrograph) both show abnormally shaped RFs. The cell identified as an RF in Fig. 4 *A* appears to be tethered to the underlying matrix at the extreme distal end of the cell process. The RF appears to have only a single, unidirectional cytoplasmic process originating from an eccentrically located nucleus. A similarly shaped RF, with an eccentrically located nucleus, is located towards the left of center in Fig. 4 *B*. It is still attached to the underlying matrix, despite a lack of cytoplasmic double contour and unidirectional cytoplasmic extension. Two other RFs, distinguishable by nuclear morphology, are located towards the right in the photomicrograph, and are free within the sinusoidal space, unattached to any underlying extracellular matrix.

Collapsed Sinusoids and Loss of Nodular Architecture. Normal LN compartmentalization is characterized by well-formed cortical sinusoids, as shown in the control group low power photomicrograph (Fig. 2 *E*). The sinusoids delimit the lymphoid parenchyma into distinct lymphoid nodules.

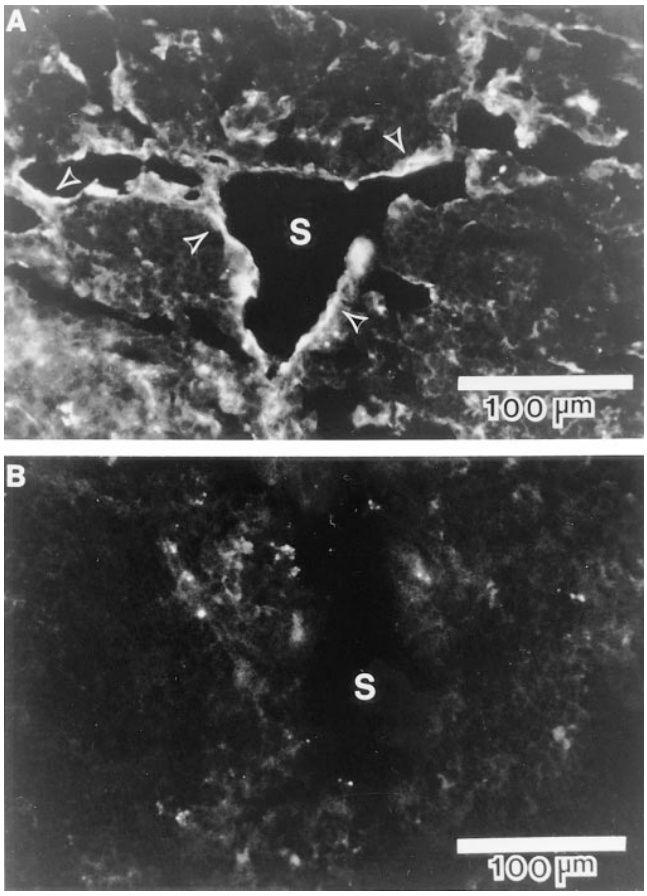

Figure 1. L1 expression by fibroblastic sinus lining cells. Immunofluorescence micrographs of 16-μm-thick frozen LN sections stained with anti–mouse L1 hyperimmune rabbit serum (*A*) or preimmune rabbit serum (*B*). *S*, Sinusoid. Note intense L1 immunoreactivity of fibroblastic sinus lining cells (*arrowheads*) compared with the low level fluorescence of lymphoid cells located in the parenchyma. *B* (negative control) is of a serial section of the same LN, including a comparable sinusoid (*S*).

During LN hypertrophy, the cell bodies of RFs extend along the sinusoidal lining to maintain a fenestrated barrier that partitions cells of the parenchyma from the sinusoidal lumen (18, 19). The extension of RFs is necessary to maintain the continuity of the cortical sinusoids with the subcapsular sinus (*Scs*, Fig. 2 *E*). L1 mAb treatment impairs RF cellular extension, preventing normal formation of cortical sinusoids and a profound loss of parenchymal nodular compartmentalization (Fig. 2 *F*). In Fig. 2 *F*, the subcapsular sinus (*Scs*) just barely begins to invaginate from the capsule, where it ends.

Macrophage Aggregation in Blind-ended Sinuses. Under normal conditions, a labyrinth of sinusoids channel lymphatic fluid and cells through the LN. Cells entering via the afferent lymphatics percolate inwards, from the subcapsular sinus to the sinusoids. In this particular immune response model, the majority of the cells trafficking into the LN from the afferent lymphatics are macrophages (Mϕs) (20). Normally, Mϕs do not form large aggregates, but are relatively evenly distributed throughout the parafollicular and medullary zones of the node. During normal immune responses, resident Mϕs are sometimes found adherent to the sinusoidal wall and, in some cases, directly anchored to reticular fibers (6). In Fig. 5 *A*, the distribution and appearance of Mϕs in normal parafollicular sinusoids is shown in an LN section from an NRIg-treated mouse.

In the L1 mAb–treated mice, the consequence of disrupting the normal remodeling of cortical sinusoids is abnormal cellular traffic and accumulation of Mϕs at apparently dead-end sinusoids. All LNs from L1 mAb–treated mice were found to contain at least one large aggregate of Mϕs (Fig. 5 *B*). Since the centrally located cells in the aggregate are not adherent to underlying matrix, they often fall out during tissue processing, creating the appearance of a false lumen (*S*, Fig. 5 *B*). By immunohistochemical analysis of serial sections for laminin (faintly present on sinusoidal walls) and CD31 (present on endothelium), the cellular aggregates were determined to be contained within sinusoids, not blood vessels (data not shown).

Functional Immune Consequences of L1 mAb Treatment. To assess the functional consequences of the architectural abnormalities, we measured several independent indices of immune function. We find that treatment with L1 mAbs does not noticeably alter primary immune responses. The battery of functional assays used are summarized in Table 2.

Normal Lymphocyte Blood Vascular Transmigration. Despite the effect of the L1 mAb treatment on the LN FRS, it did not cause any detectable morphologic change in the blood vasculature. Normal venules were identified on plastic-embedded sections stained with toluidine blue (Fig. 2, *E* and *F*) and by immunohistochemistry for laminin (Fig. 2, *C* and *D*). Since postcapillary venules are major sites of lymphocyte transmigration into activated LNs, we assayed their functional integrity by measuring the total number of lymphocytes within the LN. Moreover, we enumerated T and B lymphocyte subsets. The total number of lymphocytes and percentages of T and B lymphocyte subsets were not changed with L1 mAb treatment (Table 3). Additionally, the mean diameter of LNs from mice treated with the L1 mAb was not statistically different from the NRIg control group (Table 1). These observations strongly suggest that L1 is not essential for lymphocyte blood vascular transmigration, at least in this experimental system.

In addition, the IgG and IgM antibody responses to injected protein antigen (KLH) were not different in the L1 mAb–treated group compared with controls (Fig. 6 *A*). Also, lymphocytes taken from the draining LNs of L1 mAb–treated mice proliferated equally vigorously in response to antigen in vitro, compared with control mice (Fig. 6 *B*).

When L1 mAb treatment was tested repeatedly in an additional in vivo immune assay (delayed type hypersensitivity [DTH]), immune responses did not differ statistically from control mice (Table 2). Likewise, soluble L1 mAb used at 20 μg/ml does not affect a one-way MLR (Table 2).

Discussion

The data presented in this report provide the first in vivo demonstration of a role for L1 in LN matrix reorganization

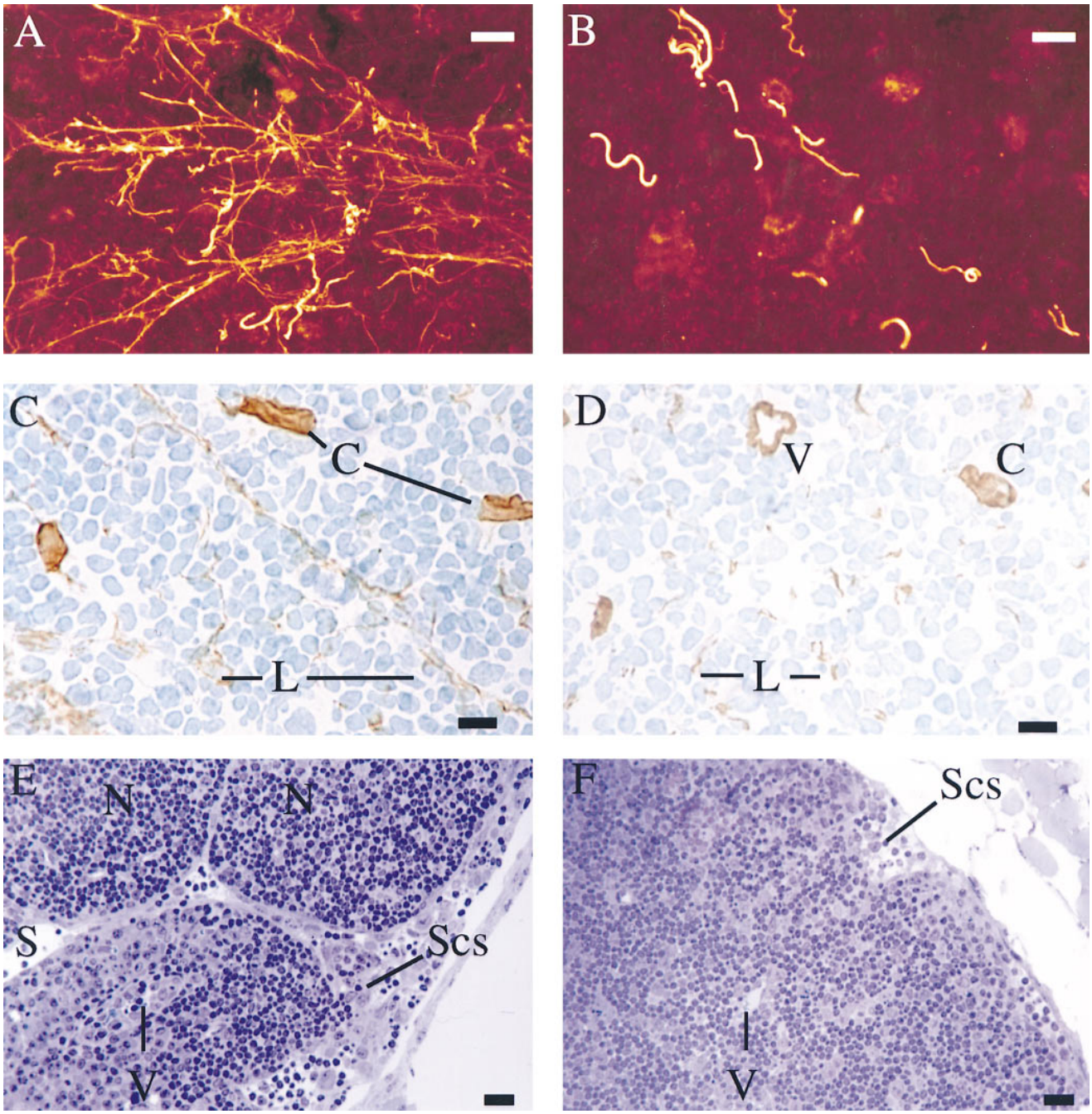

Figure 2. Histological and immunological examination of FRS architecture in immune LNs. Controls *A*, *C*, and *E* were harvested from mice injected with the NRIg. *B*, *D*, and *F* are LNs from L1 mAb–injected animals. (*A* and *B*) Stacked confocal images of LN sections cut 48 μm thick and immunostained for vimentin. The RF processes stain brightest for vimentin and appear white against the dark red background. (*C* and *D*) Photomicrographs of 6-μm-thick frozen LN sections stained for laminin by immunohistochemistry. *V*, Venules. *C*, Capillaries. *L*, Laminin. (*E* and *F*) Photomicrographs of toluidine blue–stained, 1-μm-thick, Araldite-embedded LN sections. *E* demonstrates normal compartmentalization of an NRIg-treated control LN. *N*, Lymph nodule. *V*, Venule. *S*, Sinus. *Scs*, Subcapsular sinus. *F* illustrates the loss of nodular architecture and collapse of cortical sinuses in LNs from L1 mAb–treated animals. In *F*, the structure designated with a *V* is a venule, not a tangential cut of a sinusoid, as evidenced by the erythrocytes within its lumen (not easily visible at this low power). Identical results were obtained using both NRIg and anti-class I as control antibodies in experiments used for plastic embedding. Bars, 10 μm in *A–D*, 20 μm in *E* and *F*.

during immune hypertrophy. L1 mAb administration during the course of an immune response results in collapsed sinusoids and loss of nodular compartmentalization in the draining hypertrophied LN. At the cellular level, RFs were short, plump, and often nonadherent to the underlying matrix. The loss of normal architecture is the result of an inability of the RF to elongate and envelop the reticular matrix as the LN distends. Fibroblast cell elongation is a

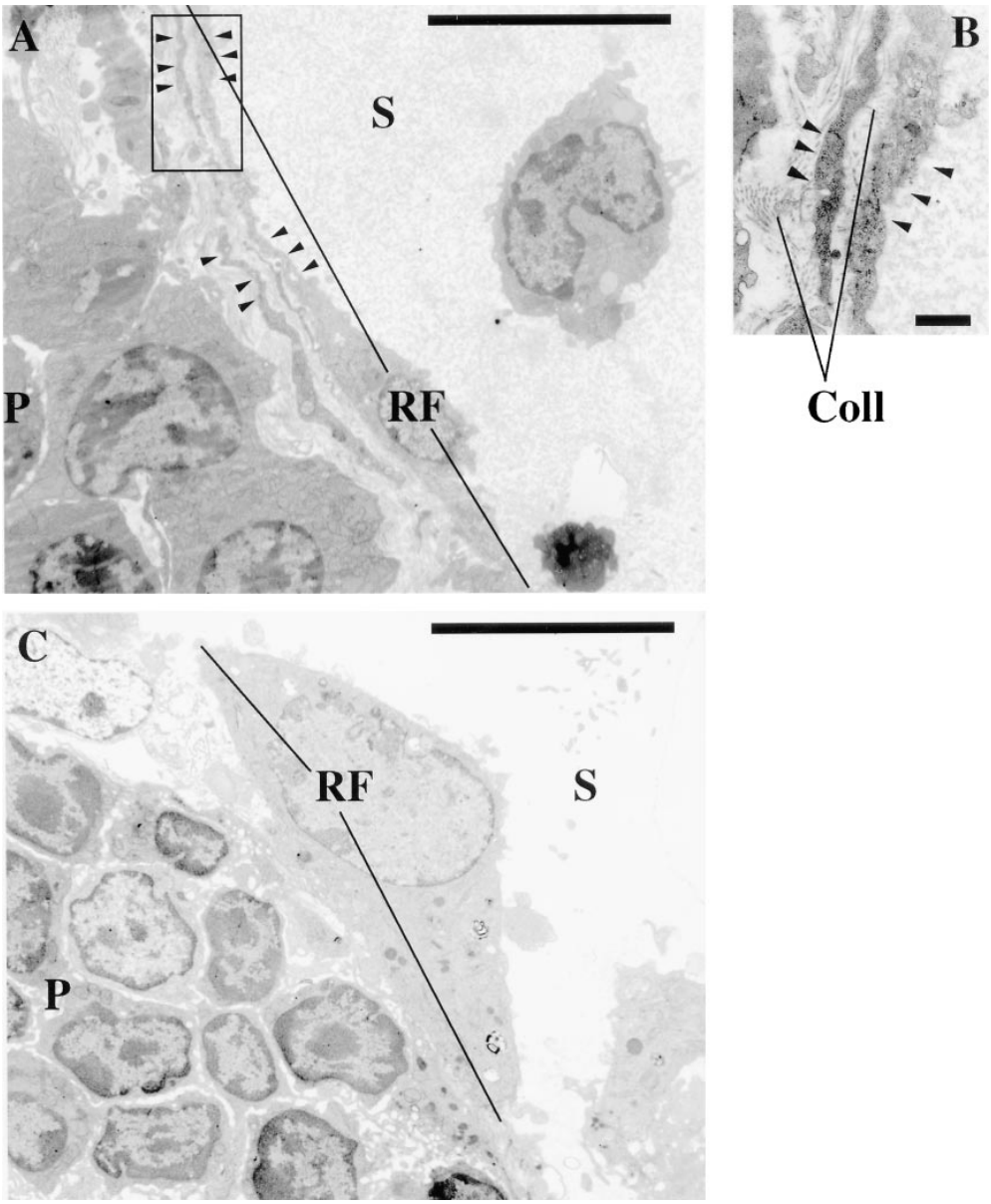

Figure 3. Transmission electron micrographs of LN cortical sinuses. The normal flattened and elongate morphology of an RF (*A*, and inset *B*) are observed in an LN from an NRIg-treated control group mouse. The RF that lines the sinusoid delimits the parenchymal compartment (*P*) from sinusoidal spaces (*S*). *B* is a high magnification of the area denoted with a box in *A*. In *B*, note the double-contour appearance (*opposing arrows*) caused by sectioning of the RF that has ensheathed collagen fibers (*Coll*). In contrast, RF from L1 mAb–treated mice (*C*) are plump rather than flattened and elongate, they lack the double-contour morphology, and they are not in close apposition to collagen fibers. Bars, 10 μm in *A* and *C*, 1 μm in *B*. The difference in mononuclear cell morphology in the parenchyma of L1 mAb–treated LNs compared with the NRIg-treated controls is not due to apoptosis (see Table 2). Similar results were obtained in three separate experiments.

necessary adaptive requirement during organ hypertrophy. To our knowledge, these experiments represent the first experimental system for the relatively selective disruption of the LN FRS, and thus may serve as a useful model to further study the function of the FRS.

L1 function is best characterized in the nervous system, where it is involved in cell motility, neurite outgrowth, axonal guidance and fasciculation, myelination, synaptic plasticity, and memory formation (for a review, see references 21–23). L1 is also expressed by numerous nonneuronal cell types, including epithelial cells (13, 14) and cells of hematopoietic origin (12). However, despite the wide expression of L1 by immune cells, there have been no published in vivo studies of L1 function in the immune system. Previous in vitro studies have demonstrated that L1 contributes to Esb-MP lymphoma binding to bend3 endothelioma cells (24), suggesting a role for L1 in lymphocyte blood vascular transmigration. L1 also accounts, in part, for the in vitro aggregation of activated splenic B lymphoblasts (12). L1 expression by follicular dendritic cells in human tonsils and by endothelial cell–associated arterioles in the red pulp of normal human spleen further suggests an important function for L1 in the immune system (25).

The effect of the L1 mAb appears specific to RFs, preventing RF elongation and attachment to the underlying matrix. Specifically, the L1 mAb does not affect lymphocyte trafficking through the postcapillary venules or immune function. Postcapillary venular function is assumed to be intact because lymphocyte influx, as gauged by the total cell number and subset quantification, is unchanged with L1 mAb administration (Table 3). Antigen-specific serum antibody and T lymphocyte sensitization are also unaffected

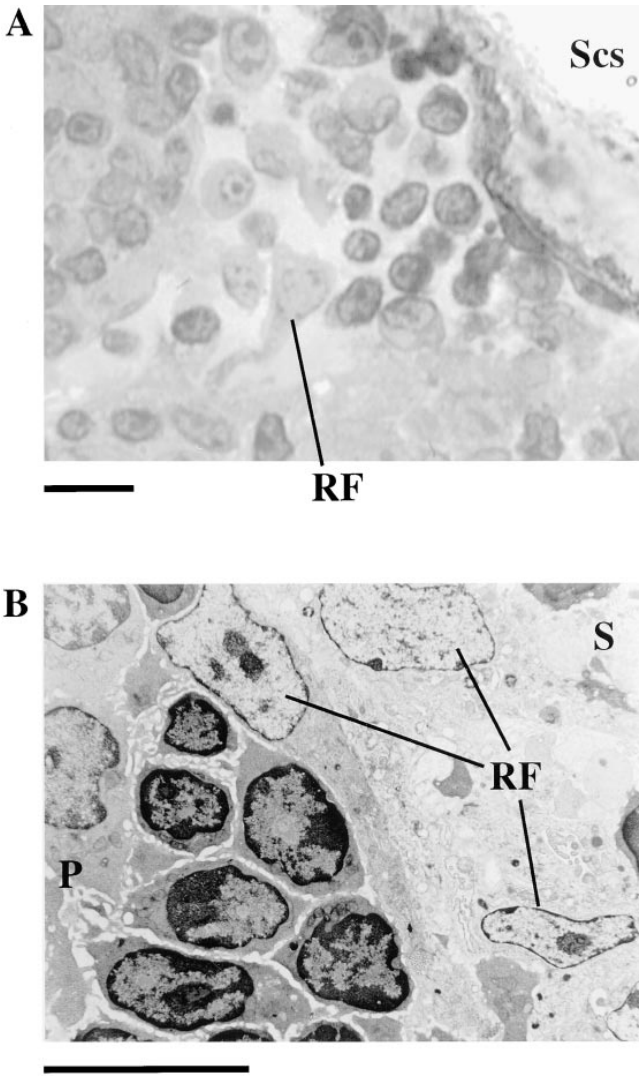

Figure 4. Sloughed RFs in sinuses of LNs from L1 mAb–treated mice. (*A*) A light photomicrograph of a plastic-embedded LN stained with toluidine blue. A malformed RF has largely detached from the sinus wall (cell labeled *RF*), tethered by a cytoplasmic process that remains attached at its end. (*B*) TEM image of three RFs, identifiable by a distinctive pattern of peripheral chromatin condensation and a large, elongated nucleus. All three RFs lack the cytoplasmic double-contour feature. The RF to the left of center has a similar abnormal, unidirectional cytoplasmic process as the RF in *A*. The two RFs in the right half of the field are not associated with collagen fibers and appear sloughed into the lumen of the sinus. *S*, Sinus. *P*, Parenchyma. *Scs*, Subcapsular sinus. Bars, 10 μm.

by the L1 mAb (Fig. 6). These pertinent negative results have been summarized in Table 2.

There are several compelling reasons suggesting that the antibody is not directly or indirectly cytotoxic to RFs. First, the antibody solution is not toxic when used at relatively high concentrations (20 μg/ml) to either 3T3 fibroblasts or lymphocyte cultures grown for 4 d in vitro (Table 2). Second, anti-L1 mAb does not induce apoptosis of lymphocytes or accessory cells, as determined by in situ TUNEL (terminal deoxynucleotidyl transferase–mediated dUTP nick end labeling) analysis of LN sections. In addition, there is no evidence suggesting that anti-L1 labels cells for antibody-dependent cell-mediated cytotoxicity or activates complement. Specifically, follicular dendritic cells and interdigitating dendritic cells are strongly $L1^+$ (reference 25, and our unpublished observations). Despite the expression of L1, repeated morphologic examination of these cell types (using the FDC-M1 and NLDC-145 mAbs, for follicular and interdigitating dendritic cells, respectively) failed to identify any demonstrable cytotoxic effects of anti-L1. Both cell number and dendritic arborization were unaffected by the anti-L1 mAb (data not shown). In addition, $L1^+$ RFs in other lymphoid organs not undergoing significant hypertrophy, such as spleen, displayed no structural alteration. If nonspecific cytotoxic mechanisms associated with antibody administration were the cause of the RF abnormality, the findings should not have been so anatomically restricted. Finally, the ultrastructural features do not suggest a cytotoxic mechanism of action. Although sloughed RFs display certain ultrastructural distinctions associated with detachment, they do not display nuclear pyknosis or karyorrhexis, features associated with cell death. These data collectively argue against the unlikely possibility that anti-L1 mAb selectively targets fibroblastic reticular cells for complement-mediated lysis or antibody-dependent cell-mediated cytotoxicity. Rather, the data are consistent with the interpretation that viable RFs slough from their matrix as a consequence of being unable to adapt to a changing substrate, as the LN undergoes rapid hypertrophy.

Based on what is known about L1, we speculate that the L1 mAb affects fibroblast function either (*a*) by inhibiting ligand binding directly involved in mechanical adhesion, or (*b*) by interfering with L1-dependent signal transduction, or a combination of both. L1 ligands that present in the LN microenvironment include laminin, L1 itself through homotypic interactions on adjacent cells, or integrins, like very late antigen-5 and the vitronectin receptor ($\alpha_v\beta_3$). Therefore, the inability of L1 expressed by RFs to bind to one or more of these ligands might directly result in an inability to elongate.

The KLH/CFA immune response model we used is characterized by an initial antigen–nonspecific, mononuclear inflammatory response at the site of subcutaneous injection. Within the first 48 h after antigen injection, antigen-bearing Mϕs and Langerhans cells migrate to the draining popliteal LN (20, 26). Our previous study on this immune response model indicated that lymphocyte influx is maximal during days 3–7 after antigenic challenge (27). Since the focus of this paper is on LN remodeling, administration of anti-L1 during this narrow time window allowed for the development of a severe architectural abnormality while simultaneously minimizing the amount of time during which an anti–rat IgG host response could occur. Therefore, this model enabled us to study events critical to matrix remodeling during the period of time when the LN enlarges 50 times its original volume.

The spleen also has fibroblastic reticular cells that express L1 (our unpublished data), but its architecture remains unaffected by anti-L1 antibody treatment. We believe this is

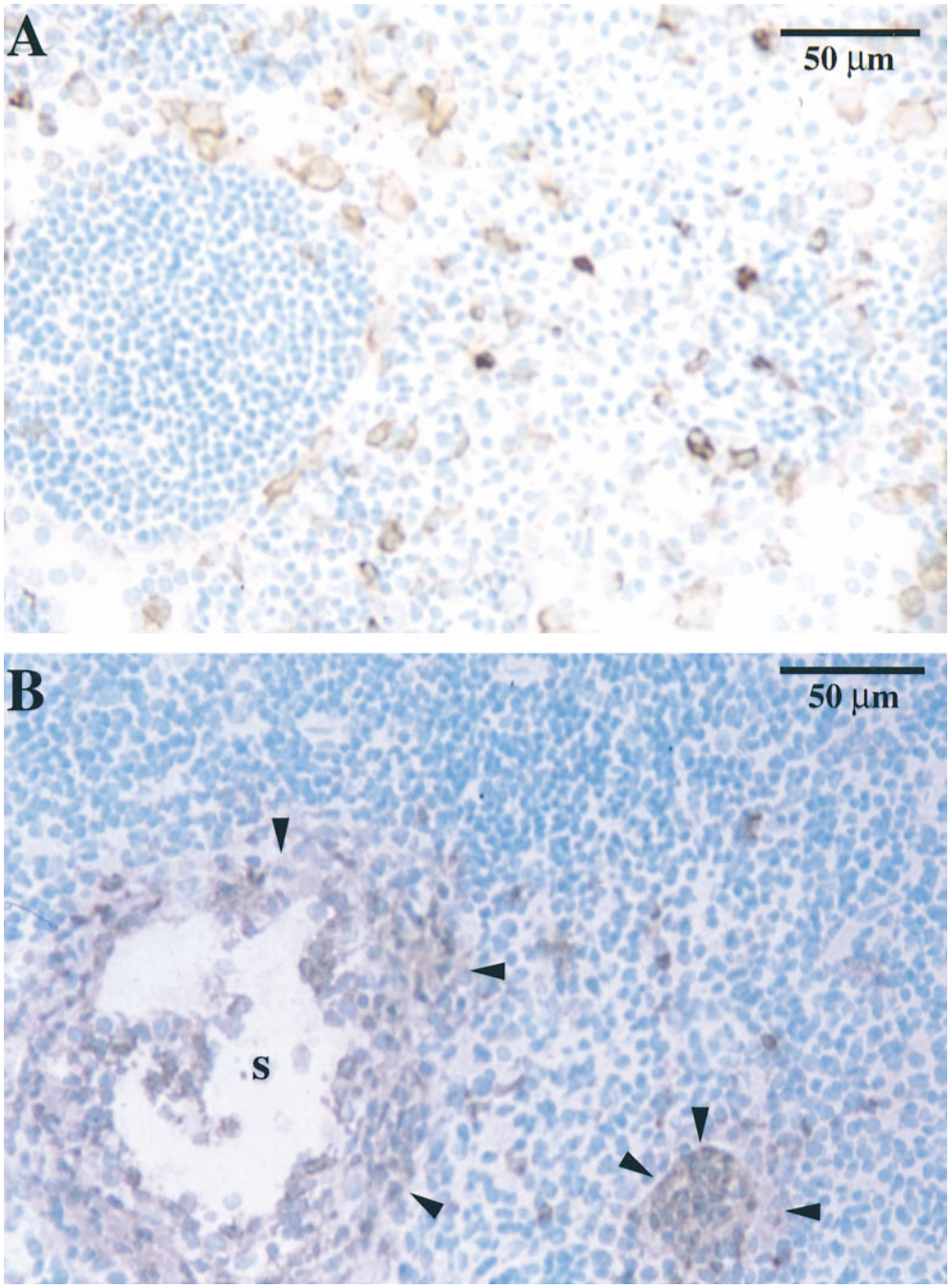

Figure 5. Immunohistochemistry staining for macrophage marker CD11b in frozen LN sections. (*A*) Representative of the normal distribution of Mϕs in the parafollicular area from an NRIg-treated mouse. Note the round follicle on the left. (*B*) Mϕ aggregates (*arrows*) are present in LNs from L1 mAb–treated mice. *S*, Space formed during histologic processing. The Mϕ aggregates in *B* are contained within malformed sinusoids.

because the spleen does not undergo a comparable degree of hypertrophy as the ~50-fold enlargement of the draining LN. In fact, our data indicate that the L1 antibody acts upon RFs only during organ remodeling. We speculate that the antibody does not directly cause detachment, but rather prevents RF reattachment to underlying matrix during cellular extension.

In terms of the functional analysis of L1 on immune cells, this battery of experiments can be viewed as the first step in characterizing this previously overlooked molecule in the immune system. We have intentionally limited our functional studies to day 7 after immunization to avoid the possibility of artifactual results associated with immune complex formation (host anti–rat IgG—rat IgG complex). In preliminary experiments, we noticed immune complex deposition in the LN vasculature in mice injected for longer time periods (2–3 wk). For this reason, we limited our studies to the effects that could be observed within only a few days after administration of the L1 mAb. Up to the seventh day after immunization (5 d after L1 mAb administration), no detectable anti–rat IgG was present in the serum (data not shown). Using anti-L1 to disrupt the FRS architecture in the KLH/CFA system, we infer that an intact LN architecture is not necessary for the evolution of

Table 2. *Summary of Assays of Lymphocyte Function Using L1 mAb*

Experiment	Result	Table
In vivo assays		
LN organ size	Normal	Table 1
Total number of LN cells and subsets	Normal	Table 3
Antigen-specific primary antibody response	Normal	Fig. 6
T cell antigen–specific sensitization	Normal	Fig. 6
In situ TUNEL assay of apoptotic foci in LN sections	Normal	Not shown
DTH	Normal	Not shown
In vitro assays		
Secondary in vitro lymphoproliferation	Normal	Not shown
One-way MLR	Normal	Not shown
NIH 3T3 proliferation with L1 mAb	Normal	Not shown

Experiments were conducted using the 324 anti-L1 mAb and control antibodies TIB 126 anti-class I, M174.4 anti–LFA-1, and NRIg. The dosage of 250 μg/mouse/d from days 2–5 consistently caused disruption of the FRS in KLH/CFA protocol. Anti-L1 antibody was also injected on days 0–5 to study potential effects of L1 in earlier immune events. This earlier administration of antibody was performed for the KLH/CFA and DTH experiments. No observed alterations in T cell sensitization, serum titers, and effector phase inflammatory responses resulted from the earlier antibody administration. In both the MLR experiments and NIH 3T3 cell proliferation assay, the 324 anti-L1 mAb and control antibodies were used at a concentration of 20 μg/ml. Proliferation was determined by [^{3}H]thymidine uptake. *TUNEL,* Terminal deoxynucleotidyl transferase–mediated dUTP nick end labeling.

primary immune responses, since no detectable differences were observed in IgM or isotype-switched IgG gamma anti-KLH–specific antibody levels, or in the level of T lymphocyte sensitization (Fig. 6).

Furthermore, since anti-L1 antibody treatment preceded KLH/CFA immunization in some functional experiments (see legend to Table 2, and Materials and Methods), it appears that the L1 molecule may not be essential to antigen presentation and early lymphocyte activation in primary immune responses.

The FRS adapts to organ distention both mechanically and at the cellular level. At the mechanical level, stretching of the reticular network is possible because LN ultrastructure is preformed before the onset of an immune response. In a study of postnatal LN development in rats, Yoshida and Takaya found that most of the gross histologic features of LN architecture are apparent by postnatal day 5, including the capsule, subcapsular sinuses, reticular fibers, and distinctive cortical and medullary zones. Furthermore, by postnatal days 16–23, reticular fibers containing elastic

Table 3. *Total LN Cell Number and Lymphocyte Subsets*

Antibody	No. LN cells	Mϕ	CD4	B220	CD8
	$\times 10^6$	%	%	%	%
Experiment 1	($n = 3$)				
L1	33 ± 12		44.0 ± 3.2	14.7 ± 3.8	13.9 ± 3.2
Class I	32 ± 3.2		46.1 ± 2.4	17.0 ± 2.2	13.9 ± 3.3
Experiment 2	($n = 4$)				
PBS	32 ± 3.7	6.2 ± 0.5	32.8 ± 0.8		
NRIg	28 ± 3.5	6.1 ± 0.4	33.8 ± 1.8		
L1	29 ± 2.5	4.8 ± 0.3	29.1 ± 0.7		
Class I	27 ± 2.8	6.0 ± 0.2	32.1 ± 0.6		
LFA-1	5 ± 1.4*	9.8 ± 0.5*	17.8 ± 1.9*		

Data represent the mean values ± SE. In both experiments, there were no statistical differences between the L1 and negative control groups as determined by ANOVA. Those antibodies injected in vivo, comprising the different experimental groups, are TIB 126 (anti–class I MHC), 324 (anti-L1), M17.4.4 (anti–LFA-1), and polyclonal NRIg. Mononuclear cell subsets were enumerated using the CD11b mAb 5C6, CD4 mAb GK1.5, 3A1/6.1 (B220), and CD8 mAb TIB 105. *Statistical significance $P < 0.001$ by ANOVA.

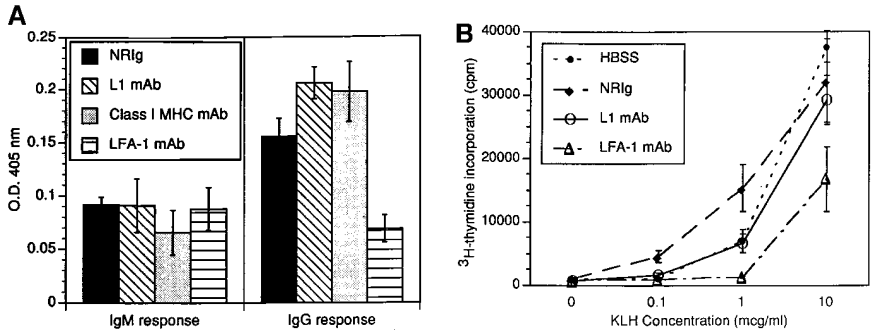

Figure 6. Primary antibody response and ex vivo lymphoproliferation to KLH/CFA. Injection of antibodies in this experiment was scheduled to precede immunization specifically to test whether anti-L1 mAb treatment could influence early events in the immune response to KLH/CFA. (*A*) Day 7, KLH-specific IgM and IgG (gamma-specific) antibody responses. L1 mAb administration does not alter the KLH-specific immune response, whereas LFA-1 mAb significantly diminishes anti-KLH IgG titers ($P < 0.001$, ANOVA). (*B*) In vivo lymphocyte sensitization is evaluated by in vitro antigen–induced lymphoproliferation. LN cells from L1 mAb–treated mice proliferate equally well as controls. Proliferation of cells from anti–LFA-1–treated control mice is significantly less ($P < 0.001$, multivariate ANOVA). In this experiment, $n = 4$ mice per group.

components were found to be ensheathed by RF cytoplasmic processes and sealed by junctional complexes (7). Therefore, the organ's blueprint is preestablished before antigenic challenge. LN hypertrophy requires extensive modification of these preset structures by the fibroblastic reticular cells.

Sinus lining cells of LNs expressed moderate levels of L1, higher than that of the surrounding parenchymal lymphocytes (Fig. 1). This is in contradistinction to the exceptionally low level of L1 on most fibroblast cell lines, such as the NIH 3T3 cell line. Previous investigators have traditionally assumed that fibroblasts such as the 3T3 cell line express nonphysiologic levels of L1 (28, 29). We are not the first to demonstrate L1 expression by fibroblasts (15). However, our data indicate for the first time that some fibroblastic cell types can express higher levels of L1 in vivo.

The mechanisms by which RFs respond to the changing environment during LN hypertrophy are unknown. One possibility is that the mechanical strain on the reticular fibers is sensed by the adherent fibroblasts through a mechanotransduction mechanism (30). Chemostimuli may also contribute to the RF response, since the immune LN is awash in cytokines, growth factors, and chemotactic factors. Scant data are presently available on the regulatory mechanism(s) controlling remodeling of the extracellular matrix by the FRS during immune responses.

We believe that this in vivo demonstration places L1 within the realm of interest to both cell biologists and immunologists. Until now, L1 has been considered primarily a neural cell adhesion molecule, of primary interest to the neurobiology community. If its function of cell extension is more generalized to other cell types, such as fibroblasts, then modulating L1 function with mAbs or genetic techniques may provide a variety of new insights in unrelated scientific areas. We speculate that the common denominator in understanding L1 function across these disparate fields is the concept of cell extension. This hypothesis is based on the observation that neurons, Schwann cells, dendritic cells of the LN, and RFs all possess the common characteristics of having an elongated shape and expressing relatively higher levels of L1. Moreover, L1 is functionally important in facilitating neuronal extension in vitro and, from this study, RF extension in vivo. Based on such analogies, we speculate that L1's shared role is likely to be found in the signaling, guidance, or maintenance of an elongate cell shape.

We thank Elizabeth Messana and Karen McNally for excellent technical assistance.

This project was funded by National Institutes of Health grant R29 AI34562.

Address correspondence to Dr. Steven A. Bogen, Department of Pathology and Laboratory Medicine, Boston University School of Medicine, Boston, MA 02118. Phone: 617-638-4103; Fax: 617-638-4085; E-mail: sbogen@bu.edu

Received for publication 22 January 1998 and in revised form 26 March 1998.

References

1. Clark, S. 1962. The reticulum of lymph nodes in mice studied with the electron microscope. *Am. J. Anat.* 110:217–257.
2. Miyata, K., and K. Takaya. 1981. Elastic fibers associated with collagenous fibrils surrounded by reticular cells in lymph node of the rat as revealed by electron microscopy after orcein staining. *Cell Tissue Res.* 220:445–448.
3. Hayakawa, M., M. Kobayashi, and T. Hoshino. 1990. Microfibrils: a constitutive component of reticular fibers in the mouse lymph node. *Cell Tissue Res.* 262:199–201.
4. Kramer, R., S. Rosen, and K. McDonald. 1988. Basement-membrane components associated with the extracellular matrix of the lymph node. *Cell Tissue Res.* 252:367–375.

5. Karttunen, T., R. Sormunen, L. Risteli, J. Risteli, and H. Autio-Harmainen. 1989. Immunoelectron microscopic localization of laminin, type IV collagen, and type III pN-collagen in reticular fibers of human lymph nodes. *J. Histochem. Cytochem.* 37:279–286.
6. Hayakawa, M., M. Kobayashi, and T. Hoshino. 1988. Direct contact between reticular fibers and migratory cells in the paracortex of mouse lymph nodes: a morphological and quantitative study. *Arch. Histol. Cytol.* 51:233–240.
7. Yoshida, T., and K. Takaya. 1992. The enveloping of intercellular collagenous fibrils by reticular cell processes in postnatal development of rat lymph nodes. *Arch. Histol. Cytol.* 55:351–359.
8. Moe, R. 1963. Fine structure of the reticulum and sinuses of lymph nodes. *Am. J. Anat.* 112:311–335.
9. Sainte-Marie, G., and F. Peng. 1986. Diffusion of a lymph-carried antigen in the filter network of the lymph node of the rat. *Cell Tissue Res.* 245:481–486.
10. Gretz, E., A. Anderson, and S. Shaw. 1997. Cords, channels, corridors and conduits: critical architectural elements facilitating cell interactions in the lymph node cortex. *Immunol. Rev.* 156:11–24.
11. Rathjen, F., and M. Schachner. 1984. Immunocytological and biochemical characterization of a new neuronal cell surface component (L1 antigen) which is involved in cell adhesion. *EMBO (Eur. Mol. Biol. Organ.) J.* 3:1–10.
12. Kowitz, A., G. Kadmon, M. Eckert, V. Schirrmacher, M. Schachner, and P. Altevogt. 1992. Expression and function of the neural cell adhesion molecule L1 in mouse leukocytes. *Eur. J. Immunol.* 22:1199–1205.
13. Thor, G., R. Probstmeier, and M. Schachner. 1987. Characterization of the cell adhesion molecules L1, N-CAM and J1 in the mouse intestine. *EMBO (Eur. Mol. Biol. Organ.) J.* 6:2581–2586.
14. Kujat, R., F. Miragall, D. Krause, R. Dermietzel, and K. Wrobel. 1995. Immunolocalization of the neural cell adhesion molecule L1 in non-proliferating epithelial cells of the male urogenital tract. *Histochem. Cell Biol.* 103:311–321.
15. Miura, M., H. Asou, M. Kobayashi, and K. Uyemura. 1992. Functional expression of a full-length cDNA coding for rat neural cell adhesion molecule L1 mediates homophilic intercellular adhesion and migration of cerebellar neurons. *J. Biol. Chem.* 267:10752–10758.
16. Nau, D. 1986. A unique chromatographic matrix for rapid antibody purification. *Biochromatography.* 1:82–94.
17. Osborn, M., E. Debus, and K. Weber. 1984. Monoclonal antibodies specific for vimentin. *Eur. J. Cell Biol.* 34:137–143.
18. Luk, S., C. Nopajaroonsri, and G. Simon. 1973. The architecture of the normal lymph node and hemolymph node. *Lab. Invest.* 29:258–265.
19. Ushiki, T., O. Ohtani, and K. Abe. 1995. Scanning electron microscopic studies of reticular framework in the rat mesenteric lymph node. *Anat. Rec.* 241:113–122.
20. Bogen, S., I. Fogelman, and A. Abbas. 1993. Analysis of IL-2, IL-4, and IFN-gamma-producing cells in situ during immune responses to protein antigens. *J. Immunol.* 150:4197–4205.
21. Schachner, M. 1993. L1. *In* Extracellular Matrix and Adhesion Proteins. T. Kreis and R. Vale, editors. Oxford University Press, Oxford. 147–148.
22. Hortsch, M. 1996. The L1 family of neural cell adhesion molecules: old proteins performing new tricks. *Neuron.* 17:587–593.
23. Fields, D., and K. Itoh. 1996. Neural cell adhesion molecules in activity-dependent development and synaptic plasticity. *Trends Neurosci.* 19:473–480.
24. Hubbe, M., A. Kowitz, V. Schirrmacher, M. Schachner, and P. Altevogt. 1993. L1 adhesion molecule on mouse leukocytes: regulation and involvement in endothelial cell binding. *Eur. J. Immunol.* 23:2927–2931.
25. Pancook, J., R. Reisfeld, N. Varki, A. Vitiello, R. Fox, and A. Montgomery. 1997. Expression and regulation of the neural cell adhesion molecule L1 on human cells of myelomonocytic and lymphoid origin. *J. Immunol.* 158:4413–4421.
26. Bogen, S., D. Weinberg, and A. Abbas. 1991. Histologic analysis of T lymphocyte activation in reactive lymph nodes. *J. Immunol.* 147:1537–1541.
27. Bogen, S., H. Baldwin, S. Watkins, S. Albelda, and A. Abbas. 1992. Association of murine CD31 with transmigrating lymphocytes following antigenic stimulation. *Am. J. Pathol.* 141: 843–854.
28. Doherty, P., E. Williams, and F. Walsh. 1995. A soluble chimeric form of the L1 glycoprotein stimulates neurite outgrowth. *Neuron.* 14:57–66.
29. Williams, E., P. Doherty, G. Turner, R. Reid, J. Hemperley, and F. Walsh. 1992. Calcium influx into neurons can solely account for cell-contact dependent neurite outgrowth stimulated by transfected L1. *J. Cell Biol.* 119:883–892.
30. Ingber, D. 1997. Tensegrity: the architectural basis of cellular mechanotransduction. *Annu. Rev. Physiol.* 59:575–599.